



CHORUS

This is the accepted manuscript made available via CHORUS. The article has been published as:

Random fiber networks with inclusions: The mechanism of reinforcement

M. R. Islam and R. C. Picu

Phys. Rev. E **99**, 063001 — Published 19 June 2019

DOI: [10.1103/PhysRevE.99.063001](https://doi.org/10.1103/PhysRevE.99.063001)

Random fiber networks with inclusions: the mechanism of reinforcement

M.R. Islam and R.C. Picu¹

Department of Mechanical, Aerospace and Nuclear Engineering, Rensselaer Polytechnic Institute, Troy, NY 12180

Abstract

The mechanical behavior of athermal random fiber networks embedding particulate inclusions is studied in this work. Composites in which the filler size is comparable with the mean segment length of the network are considered. Inclusions are randomly distributed in the network at various volume fractions and cases in which fibers are rigidly bonded to fillers, and in which no such bonding is imposed are studied separately. In presence of inclusions, the small strain modulus increases, while the ability of the network to strain stiffen decreases relative to the unfilled network case. The reinforcement induced by fillers is most pronounced in sparse networks of floppier filaments that deform in the bending-dominated mode in the unfilled state. As the unfilled network density or the bending stiffness of fibers increase, the effect of filling diminishes rapidly. Fillers lead to a transition from the soft, bending-dominated, to the stiffer, [stretching-dominated](#), deformation mode of the network, transition which is primarily responsible for the observed overall reinforcement. The confinement, i.e. the restriction on network kinematics imposed by fillers, causes this transition. These results provide a justification for the observed difference in reinforcement obtained in sparsely versus densely cross-linked networks at given filling fraction, and provide guidance for the further development of network-based materials.

Keywords: soft composites, collagen, fiber networks, reinforcement

¹ Corresponding author. Tel: 1 518 276-2195, E-mail: picuc@rpi.edu.

1. Introduction

Many soft materials have a random fiber network as their primary structural component. Examples include the cellular cytoskeleton [1], the extracellular matrix (ECM), various connective tissues [2], and biomaterials such as mycelium [3], as well as synthetic materials such as paper [4], non-wovens [5], rubber [6] and hydrogels [7]. In general, network-based materials are heterogeneous and often contain inclusions with dissimilar mechanical properties. For example, hydrogels reinforced with nanoparticles [8], particle-filled collagen scaffolds [9-11], and mycelium network embedding particles [12] are some prominent examples. In all these systems, inclusions influence the deformation mechanisms and the stress distribution in the underlying network, thus affecting critically the macroscopic behavior of the material. Despite the prevalence of such examples, a fundamental understanding of how inclusions alter the mechanical properties of the underlying network remains elusive, which limits our ability to design filled network based materials.

The mechanics of fiber networks has been an active research area for more than a decade [13-16]. Most fiber networks of practical importance are sub-isostatic (i.e. their average connectivity is below the threshold defined by the Maxwell criterion for structures of trusses [17]) and predominantly derive rigidity at small strains from fiber bending [18,19]. Sub-isostatic networks acquire non-zero stiffness in presence of residual stresses [20] or upon straining [21]. Network elasticity is controlled by fiber density, degree of cross-linking and fiber **stretching** and bending rigidities [18,19,22]. Dense networks with fibers relatively stiff in bending deform (approximately) affinely and store strain energy mostly in the **stretching** deformation mode of fibers. Office paper, densely cross-linked non-wovens and some textiles are examples of this type of network. Low density and/or sparsely cross-linked networks, as well as networks of fibers soft in bending, deform in a highly non-affine manner, storing energy mostly in the softer, bending deformation mode of fibers. Most biological networks belong to this class of structures. Experimental and theoretical works have also shown that networks stiffen with increasing strain, which results in ‘J shaped’ stress-strain curve [23,24]. This nonlinear behavior is geometric in nature, being primarily associated with the re-orientation of fibers, or fiber segments, during loading [25], and, in relatively sparsely crosslinked networks, is less due to the nonlinearity of the individual fiber constitutive behavior [26]. Therefore, strain stiffening is highly dependent on network architecture [27].

Reinforcement of man-made networks with fillers has been used technologically for a long time, while biological tissue also contains “inclusions” such as cells and proteoglycans. Furthermore, nanoparticles are embedded in the cellular cytoplasm [28] or in the extracellular matrix [29] and used to apply loads (when moved using external fields) or as tracers of deformation. The effect of such inclusions on the stiffness and rheology of the embedding medium is still a matter of debate.

The effect of fillers on network stiffness is different in densely and sparsely cross-linked cases. Particulate-filled epoxies exhibit modest stiffness enhancement upon filling with nanoscale or microscale particles [30]. Reinforcement of athermal collagen structures with nanofillers produces much stronger effects [9-11].

To explore the effect of fillers in fibrous materials, we consider in this work three-dimensional (3D) models of random athermal fiber networks containing spherical rigid inclusions of radius comparable to the mean segment length of the network. These are relevant for cases in which the network behavior is primarily enthalpic, including filled non-wovens of various kinds and connective tissue composed from largely athermal collagen or/and elastin filaments. The inclusions are caged by the network and are rigidly bonded to the fibers they contact. The slippery interface case is also considered in separate simulations. We explore the effect of the filler volume fraction on the linear and non-linear components of the mechanical response of networks loaded in tension. We observe that the addition of fillers has large effect if the base network is sparsely cross-linked or/and it is composed from filaments which have soft bending deformation modes. On the other hand, the reinforcement effect is weak in dense networks. We show that fillers have a strong confining effect on the surrounding network, whose dominant deformation mode changes to the stiffer [stretching](#) mode. This transition is responsible for the increase of the small strain modulus and the reduction of the ability of the network to strain stiffen under large deformations. The model definition is presented in the next section. In the results section we discuss the generic effect of fillers on network behavior, describe a cross-over from the bending to the [stretching](#) deformation mode as the filler volume fraction increases, and explore the mechanism responsible for the observed reinforcement effect.

2. Models and methods

To model the discrete fiber network with embedded inclusions, a 3D network of straight fibers, each of length L_0 , is constructed using a procedure similar to that developed previously [27]. In

this approach, sparse fiber assemblies are generated first based on the random sequential adsorption (RSA) algorithm where fibers of length, L_0 , are deposited sequentially with random spatial location and orientation in the cubic domain while satisfying non-overlapping constraint. Six such fiber assemblies are generated and placed around the final model domain, similar to the method of fiber packing described in ref [31]. Dynamic finite element (FE) simulations are subsequently performed to pack the fibers of all six assemblies within the specified cubic volume of the model, V . Fibers are represented using Timoshenko beam elements during this packing process, and surface-based contact interaction are enforced to satisfy non-overlapping constraint [31].

Next, fiber-to-fiber crosslinks are introduced at locations where the inter-fiber distance is smaller than $2d$, where d is the fiber diameter. After the cross-linking process, fibers not cross-linked to the network and fiber dangling ends are removed such to obtain a fully crosslinked fiber network, as shown in Fig. 1(a). The size of the model, $V^{1/3}$, is at least three times larger than L_0 such to reduce the model size effect. In the remainder of this paper, we refer to this model (Fig. 1(a)) as ‘the unfilled network.’

To introduce inclusions within the unfilled network, spherical inclusions are placed randomly inside the cubic domain and fibers are trimmed at their intersection with inclusions. Finally, fiber-to-inclusion cross-links are introduced to obtain a fully connected structure, as shown in Fig. 1(b). Figure 1(c) shows the discrete interface between an inclusion and the surrounding fibers. The fiber-inclusion cross-links are of the same nature with those between fibers and transmit both forces and moments (are of ‘welded’ type).

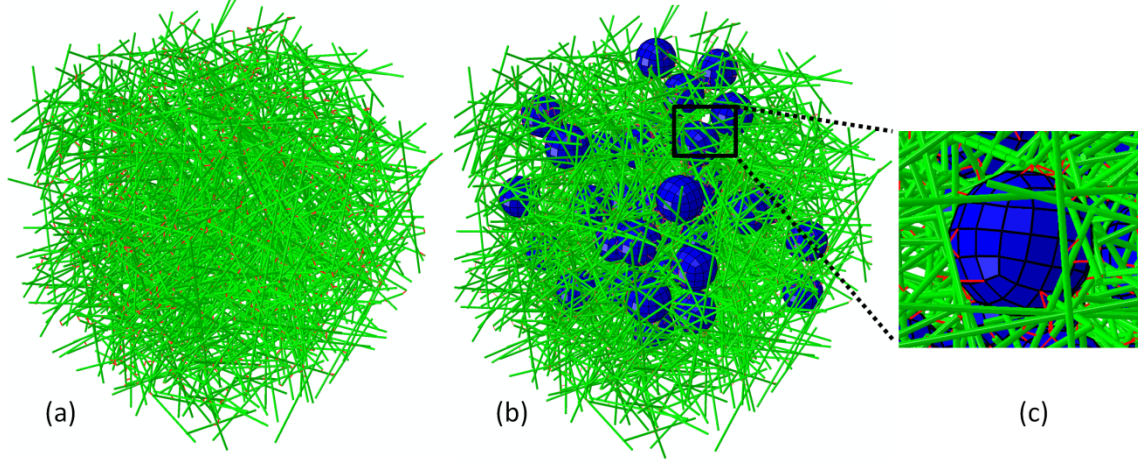


Figure 1. (a) 3D crosslinked fibrous network. (b) The network in (a) filled with spherical inclusions. The fillers occupy $\phi = 5\%$ of the model volume in this realization. (c) Zoomed view of the discrete interface between an inclusion and surrounding network. The green lines represent fibers, red lines mark the cross-links and the blue spheres are inclusions (color online).

The important network parameters are the network volume fraction, ρ_v , and the fiber properties. ρ_v is related to the network density (defined as the total length of fiber per unit volume) ρ , as $\rho_v = \rho A$, where A is the cross-sectional area of fibers. **All fibers in the model have the same length, L_0 , which is taken here to be the unit of length and hence, it is used as normalization factor for all length.** Segments between neighboring cross-links along given fiber have length l ; this quantity is Poisson distributed and the mean segment length is denoted by l_c . The mean number of cross-links per fiber (n_c) is $n_c = L_0/l_c + 1$. In the models used in this study, $n_c \approx 5$, and the network density ρ is kept constant at $\rho L_0^2 = 103.2$, with $\frac{l_c}{L_0} = 0.25$.

The fiber material is considered linear elastic, with Young's modulus E_f . The fiber bending and axial rigidities are proportional to $E_f I$ and $E_f A$, respectively, where I is the axial moment of inertia of the fiber cross-section. We consider fibers with circular cross-section; networks of fiber with non-circular cross-section present additional complexities associated with the existence of two principal bending modes [32]. It has been determined earlier [18,22,33,34] that the mechanical behavior of networks formed by filaments of same type depends on the fiber bending and axial rigidities exclusively through a parameter with units of length, $l_b = \sqrt{E_f I / E_f A}$. For fibers with

circular section $l_b = d/4$. We note that if the filaments cannot be considered beams, l_b simply represents the ratio of the bending and axial rigidities and is not necessarily linked to any geometric parameter of the fiber cross-section. We take this view in the present work and vary l_b/L_0 in the range 10^{-4} to 0.15.

Fillers are defined by their diameter, D , and their volume fraction ϕ . Parameter ϕ , computed as the total volume of inclusions divided by the model volume, V , is varied in the range 2% to 10%. The filler diameter is taken to be $D = 2l_c$ in all models and all inclusions in given model are of same size. Inclusions much smaller than l_c are also smaller than the typical inter-fiber distance and are likely in contact with a single fiber. Their reinforcement is likely limited. If $D \gg 2l_c$, the network appears as a continuum on the scale of the inclusion and the standard view of a particle-filled continuum applies [35]. We expect that interesting behavior emerges when the scale of the filler, D , is comparable with the characteristic length scale of the network, l_c . This motivates the present choice of parameters.

Inclusions are considered rigid. This represents all situations in which fillers are much stiffer than the surrounding network/matrix, such as electrospun network filled with nanoparticles [36], epoxy filled with nanoparticles [37], or reconstructed collagen networks with nanofillers [9-11].

Fibers are discretized with Timoshenko beam elements of aspect ratio 5. Inclusions are modeled using rigid shell elements (approximately 300 elements per inclusion). The excluded volume constraints between fibers and between fibers and inclusions are enforced using the general contact algorithm in Abaqus [38]. All cross-links, between fibers and between fillers and fibers, are modeled using rigid connector elements which are not allowed to fail. The model is deformed uniaxially in tension by imposing equal and opposite displacement boundary conditions on two opposite boundaries. Traction free boundary conditions are imposed on model surfaces parallel to the loading direction. These are also constrained to remain planar during deformation. The model is free to contract in the direction transverse to the loading. The solution is obtained using the finite element solver Abaqus/Explicit (version 6.13-1).

3. Results and discussion

3.1 Reinforcement depends on the type of network used as matrix

Figure 2 shows the tensile stress-stretch response of filled networks with four inclusion volume fractions, $\phi = 2\%, 5\%, 8\%$ and 10% . Figure 2(a) shows curves for systems in which the unfilled network deformation is non-affine, with $l_b/L_0 = 0.008$ while Fig. 2(b) corresponds to cases in which the unfilled network deformation is approximately affine, with $l_b/L_0 = 0.04$. The stress-stretch curves of the corresponding unfilled networks are also shown for reference. The stress measure used in this work is the nominal (first Piola-Kirchoff) stress, S and the deformation measure used is the stretch ratio, λ . The reported stress is normalized by the fiber modulus, E_f , which is considered here the unit of stress.

It is observed that inclusions stiffen the network and the effect increases with increasing ϕ . Both filled and unfilled networks demonstrate three distinct regimes during uniaxial deformation, which are identical to those usually observed for unfilled networks [27]. The deformation is linear elastic (of modulus E_0) in the first regime, for $1 < \lambda \leq 1.05$. Beyond this critical stretch ($\lambda_{c1} \sim 1.05$), a second regime is observed in which strain stiffening is pronounced. Strain stiffening is primarily due to the gradual orientation of fibers in the loading direction. Fibrous networks of small l_b/L_0 values strain stiffen quadratically, i.e. $S \sim (\lambda - 1)^2$ [27]. In the third regime, the stress-stretch curve becomes linear again. In this regime, multiple stress paths form and transmit loads across the sample, while the majority of fibers are not loaded. In most applications (e.g collagen networks in connective tissue) the network functions in regimes I and II. Networks with large l_b/L_0 , which deform mostly in the **stretching** mode, exhibit little strain stiffening up to large stress values. The three regimes are visible in Fig. 2(a) for cases with low l_b/L_0 , while the stress-strain response is approximately linear throughout the entire strain history in Fig. 2(b). The arrows in Fig. 2(a) indicate the transition between regimes I and II and between regimes II and III for the unfilled network (black arrows) and the filled network with $\phi = 10\%$ (red arrows). **The transitions between these three regimes are better visualized when the stress-stretch curves of Fig. 2(a) are replotted as tangent stiffness vs. stress, as shown in Fig. 2(c). The normalized tangent stiffness is calculated as $E_t/E_f = d(S/E_f)/d\lambda$. The initial linear regime appears as a plateau at small stress values in Fig. 2(c).**

We observe that the stretch at the first transition, λ_{c1} , is largely unaffected by the presence of inclusions, while the second transition, λ_{c2} , depends on the filling fraction. λ_{c2} decreases with increasing ϕ and hence the range of stretch ratios corresponding to regime II decreases with increasing ϕ (see Fig. S1 of the Supplementary material). A more detailed discussion of this aspect is deferred to section 3.3.

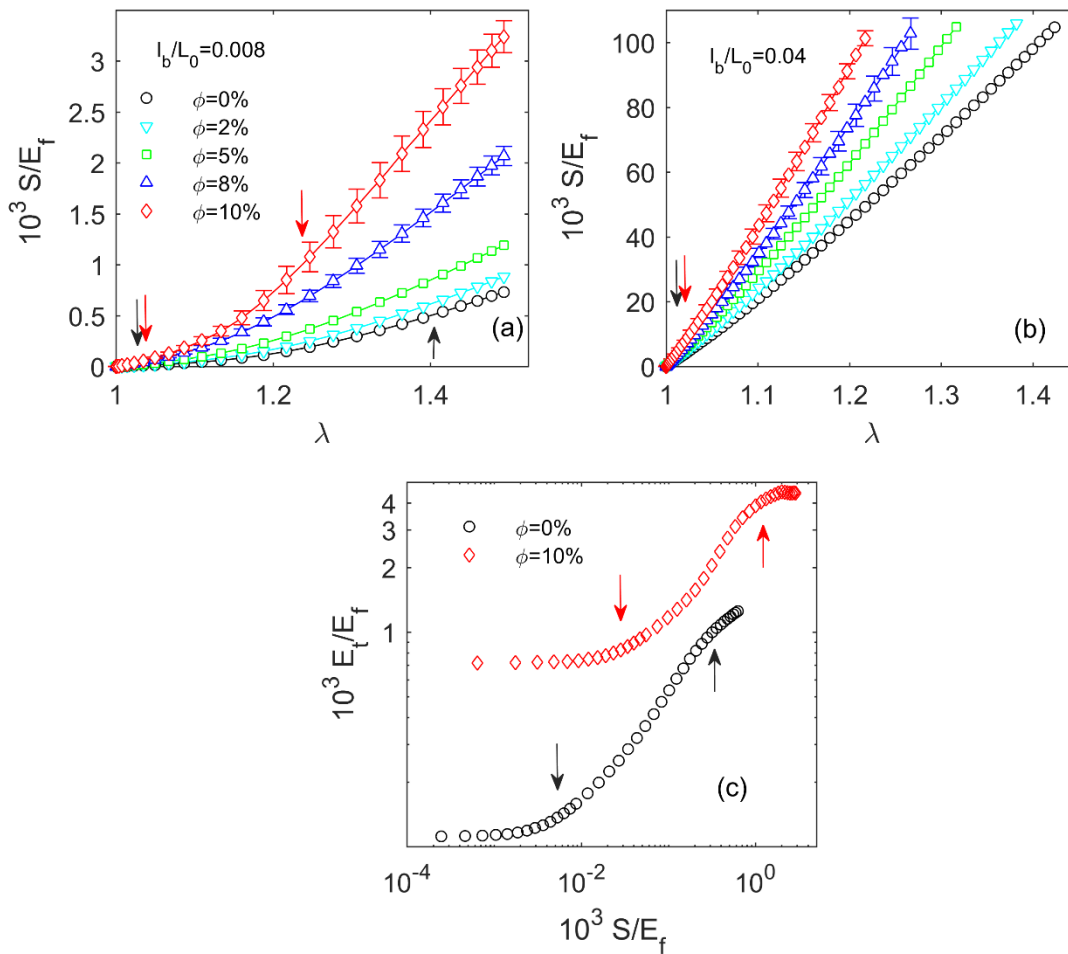


Figure 2. Nominal stress versus stretch curves for fiber networks with rigid inclusions: (a) corresponds to $l_b/L_0 = 0.008$ and (b) corresponds to $l_b/L_0 = 0.04$ Results for four inclusion volume fractions, ϕ , are reported. The stress-stretch curve of the unfilled network, $\phi = 0\%$, is shown for reference. Each curve is obtained by averaging the response of three realizations of same network parameters. The bars shown for $\phi=8\%$ (red diamonds) and $\phi=10\%$ (blue upward triangles) represent the range of the three realizations. The bars are not shown for the other curves for which the range of variability is comparable to the size of the symbols. The arrows in (a) indicate transitions between the three regimes of deformation for the unfilled network (black

arrows) and the filled network with $\phi = 10\%$ (red arrows). The curves corresponding to $\phi=0$ and 10% from (a) are replotted in (c) as tangent stiffness versus stress. This representation outlines better the three regimes described in the text, and the transition points between them (marked by arrows).

The effect of filling is discussed further in terms of the linear elastic modulus and strain stiffening. Figure 3(a) shows the variation of E_0 as a function of l_b/L_0 for filled networks with various inclusion volume fractions, ϕ . The vertical axis is normalized by the affine modulus of the unfilled network, E_{affine}^{uf} . Data for unfilled networks, E_0^{uf} (black circles), is shown for comparison. The effective modulus E_{affine}^{uf} is evaluated by assuming that each filament deforms affinely with the imposed macro-deformation, which restricts their deformation to the **stretching** mode, leading to $E_{affine}^{uf} = \beta\rho E_f A$. As well-known [39], the affine modulus scales linearly with the density and is proportional to $E_f A$. The constant β depends on the network architecture and, for the models considered here, $\beta = 0.12$. The plot exhibits the two distinct regimes (defined approximately by the vertical dashed line in Fig. 3(a)) broadly discussed in the literature on fiber networks [14,18,19] and reviewed in the introduction: the modulus approaches the affine prediction at large l_b/L_0 and $E_0^{uf} \sim E_f A$, while at small l_b/L_0 , $E_0^{uf} \sim E_f A l_b^2 = E_f I$, the deformation is non-affine and the bending deformation mode of fibers prevails.

Filled networks exhibit qualitatively the same general behavior, but with important distinguishing differences. The transition from the **stretching-dominated** to the bending-dominated regimes takes place at smaller values of l_b/L_0 as ϕ increases. The transition is also broader and in this regime one can approximate $E_0(\phi) \sim E_{affine}^{uf} l_b^{2\alpha} \sim (E_f A)^{1-\alpha} (E_f I)^\alpha$, where $\alpha = f(\phi) < 1$. The exponent α varies from 0.99 ($\phi = 2\%$) to 0.695 ($\phi = 10\%$) in the given range of filler density. This implies that, at given l_b/L_0 , the contribution of the **stretching** deformation mode to the small strain modulus increases with ϕ . This issue is discussed further in section 3.2.

Fillers reinforce the network in all cases and hence $E_0(\phi) > E_0^{uf} = E_0(0)$. However, reinforcement is much more pronounced in the bending-dominated regime. To emphasize this result, the data in Fig. 3(a) is re-plotted in Fig. 3(b) by normalizing the filled network modulus with the modulus of the corresponding unfilled network, i.e. $E_0(\phi)/E_0^{uf}$. While in the **stretching-**

dominated regime the modulus increases by a factor of ~ 3 upon the addition of up to 10% volume fraction of rigid fillers, in the bending-dominated regime the reinforcement is more than one order of magnitude larger. This is the first important result of the present work.

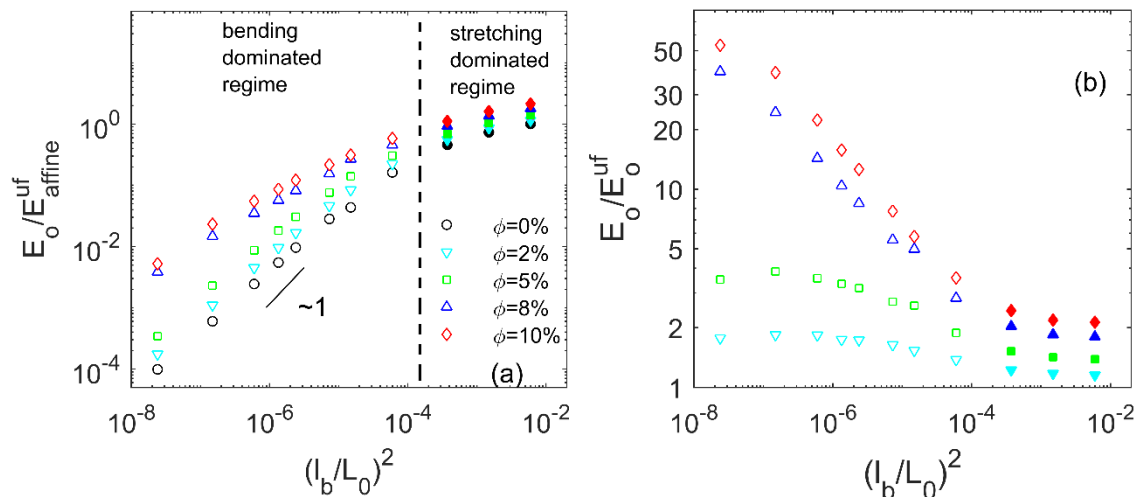


Figure 3. (a) Scaling of the small strain modulus (E_0) of filled networks with l_b/L_0 for different filler volume fractions, ϕ . The vertical axis is normalized by the affine modulus of the unfilled network, E_{affine}^{uf} . The vertical dashed line indicates approximately the transition from bending (unfilled symbols) to **stretching** (filled symbols) dominated network response for the unfilled networks. The transition shifts gradually to the left as ϕ increases. (b) Data in (a) replotted as $E_0(\phi)/E_0^{uf}$ function of l_b/L_0 .

Figure 4 compares the reinforcement observed experimentally in two types of nanocomposites: epoxy filled with nanoparticles and filled reconstructed collagen and fibrin networks. Epoxies are densely cross-linked networks in which the strands are rather stiff in bending. Elasticity is enthalpic in these systems. The data is presented as $E_0(\phi)/E_0^{uf}$ (i.e. the reinforcement) versus the filling fraction (vol%). The domain representing filled epoxies is based on experimental data from [30,37]. The figure includes data for several collagen-based composites incorporating hydroxyapatite whisker particles [11], Al_2O_3 - ZnO_2 nanoparticles[9], and polyacrylic acid nanoparticles [10], in which the collagen is in the usual fibrillar form, as well as data from a study of fibrin networks embedding platelets [40]. The two data sets separate in the vertical direction, with the reinforcement of the sparsely cross-linked networks of flexible strands being much more pronounced. The results from Fig. 3(b) are also shown, for $l_b/L_0 = 3.8 \times 10^{-3}$ and 3.8×10^{-2} .

As discussed above, the reinforcement obtained in a network of flexible fibers is much larger than that of a network of fibers stiff in bending filled with the same volume fraction of rigid fillers.

It is further of interest to compare the reinforcement observed here with that expected for a particulate composite with continuum matrix of stiffness identical to the stiffness of the corresponding unfilled network. To this end, we add to Fig. 4 predictions for the continuum equivalent composites obtained with the generalized self consistent method [41]. These continuum-based models are based exclusively on the filler volume fraction and predict lower reinforcement than both network models and most of the experimental values for all ϕ . This difference has at least two sources: (i) network models are intrinsically heterogeneous and do not deform exactly affinely even at large values of l_b/L_0 ; (ii) Classical local continuum models with no internal length scale are not adequate to represent the deformation of fiber networks at a scale comparable with the fiber segment length. Non-local formulations that take into account the micropolar nature of stress in these structures are more appropriate [42]. Furthermore, we expect that networks filled with inclusions of size much larger than any internal length scale of the network (l_c, L_0) would exhibit behavior closer to that predicted by the equivalent continuum models. The numerical data in Fig. 4 also indicate that the effective modulus scales linearly with the filling fraction in this range of ϕ , which is expected based on continuum mechanics results [41].

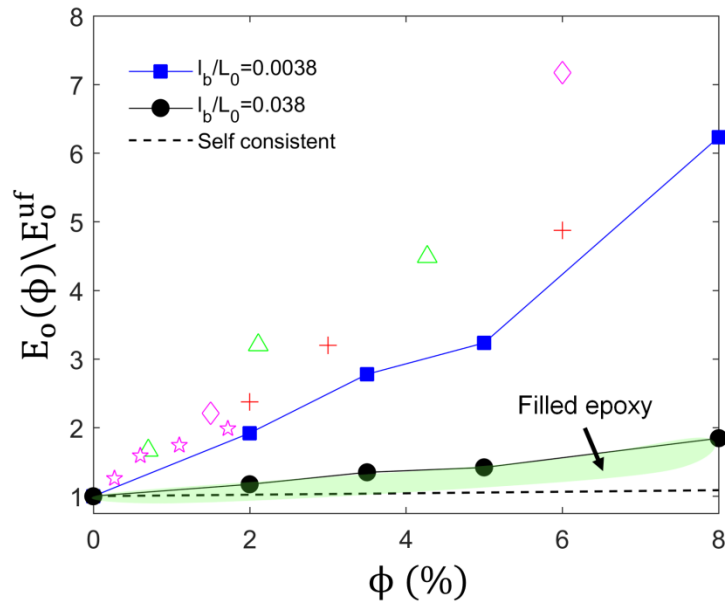


Figure 4. The degree of reinforcement $E_0(\phi)/E_0^{uf}$ function of the volume fraction of rigid fillers, ϕ , as predicted by the present network models with two values of l_b/L_0 , from Fig. 3(b) (lines with filled symbols), and by the generalized self-consistent scheme for continuum composites (dashed line). Data for different collagen-based composites reinforced with hydroxyapatite particles (plus symbols) [11], Al_2O_3 -ZnO nanoparticles (open pentagon symbols) [9], and polyacrylic acid nanoparticles (open triangle symbols) [10] and fibrin network with embedded platelets (diamonds)[40] are shown. The shaded domain represents the range of reinforcement values reported for filled epoxy materials based on data from [37].

The observation that low density networks of filaments soft in bending change their small strain modulus by orders of magnitude upon the addition to the network of a small fraction of rigid filaments has been made before using two-dimensional models [43]. In this work, Mikado models with bending-dominated and [stretching-dominated](#) deformation were considered and a small fraction of very stiff fibers were added. The overall modulus of the composite structure increased by more than 2 orders of magnitude in the case of the bending-dominated base networks, even before the reinforcing fibers were dense enough to produce a percolated sub-network of stiff filaments. This effect is associated with the fact that stiff filaments restrict the deformation of the base network filaments with which they come in contact to the [stretching](#) deformation mode. The effect is more pronounced as the non-affinity of the base network increases. A similar stiffening effect was reported in [44] for 2D models, but was not observed in the 3D models reported in [45]. The discussion in [43] is limited to the small strain modulus of the composite network and does not address the non-linear behavior of the material.

It is of interest to discuss the effect of inclusions on the larger strains, non-linear behavior of filled networks. To facilitate the direct comparison of curves corresponding to different filling fractions, we normalize the stress with the small strain modulus of the respective filled network and plot in Fig. 5(a) the normalized stress, S/E_0 , versus stretch for networks with $l_b/L_0 = 8 \times 10^{-3}$. As ϕ increases, strain stiffening becomes less pronounced. The data in Fig. 5(a) are replotted in Fig. 5(b) as tangent stiffness versus stress. The normalized tangent stiffness $E_t/E_0 = d(S/E_0)/d\lambda$ is equal to 1 at small strains by definition. Networks enter the strain stiffening regime II at a critical stretch λ_{c1} which is approximately ϕ -independent (Fig. S1). Since E_0 increases with ϕ , the

transition appears shifted to larger stresses in this representation as indicated by the arrows (shown for $\phi=0\%$ and 8% only). The unfilled network stiffens in regime II as $S \sim (\lambda - 1)^2$, as also observed in [27]. Filled networks exhibit similar stiffening. While the regime I to II transition is rapid in the case of unfilled networks, it is more gradual in filled networks of larger ϕ . In addition, the transition from regime II to III takes place at smaller stretches, λ_{c2} , for the filled networks (Fig. S1). This renders regime II less well defined in the filled networks case, which leads to the appearance of weaker non-linear behavior seen in Fig. 5(a).

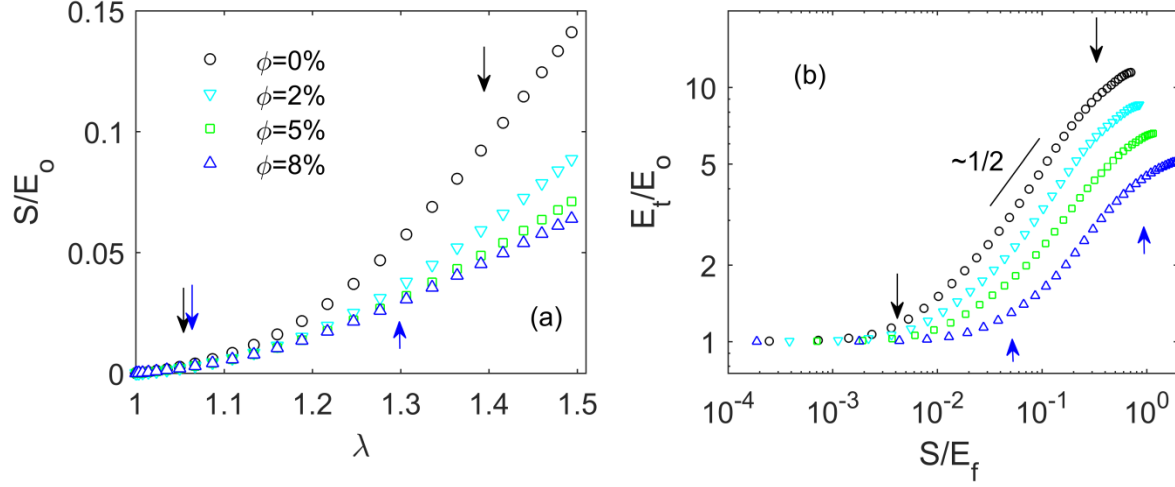


Figure 5. (a) Data from Fig. 2(a) normalized such to emphasize the effect of ϕ on the non-linear component of the stress-stretch curves. (b) shows the curves in (a) represented as tangent stiffness versus stress such to emphasize the three regimes of deformation and the differences of strain stiffening in filled and unfilled networks.

3.2 Filler-controlled transition from bending to **stretching-dominated** deformation

The transition of the dominant deformation mode of fibers from the **stretching** to the bending mode as either or both the network density decreases or fibers become softer in bending (l_b decreases) is well documented in the literature [46,47]. Here we show that a similar transition takes place when the filler volume fraction increases. Specifically, when a bending dominated network is reinforced with increasing volume fractions of rigid fillers, it stores gradually more energy in the stretching deformation mode of fibers. This effect is demonstrated in Fig. 6 for a network with $l_b/L_0 = 8 \times 10^{-3}$. The curves represent the fraction of the total strain energy stored in the **stretching** and bending modes. The other deformation modes (torsion and shear) store less than 5% of the strain energy in all cases. The unfilled network stores more than 80% of the strain energy

in the bending mode. As deformation proceeds, the two fractions become comparable and eventually the stretching mode becomes dominant. The transition takes place at $\lambda \sim 1.2$, which corresponds to the middle region of regime II of the stress-stretch curve in Fig. 2(a). As ϕ increases, the fraction of strain energy stored in the bending mode at small strains decreases and the stretch at which the modes switch dominance decreases. The network with $\phi = 10\%$ is stretching-dominated almost throughout the entire deformation history. This indicates that fillers constrain the deformation of fibers in their neighborhood to deform in the **stretching** mode. This effect was also discussed in [43] in the context of 2D Mikado networks and its mechanistic origins are further analyzed in section 3.3. The observation that the deformation mechanism of the network is modified by the presence of inclusions is the second important conclusion of this work.

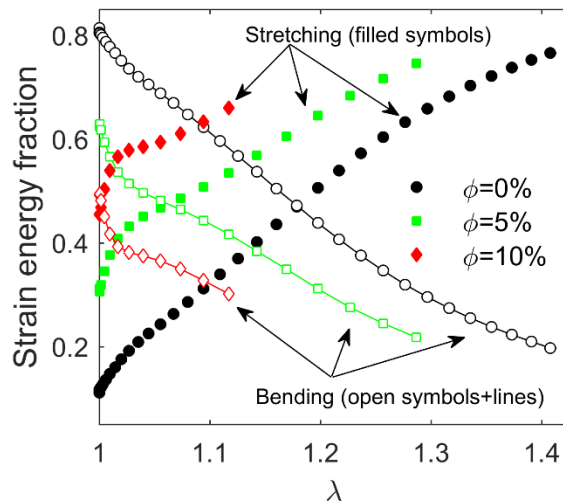


Figure 6. Evolution of energy partition with stretch for a network with $l_b/L_0 = 8 \times 10^{-3}$ and at different filler volume fractions, ϕ . For each case, only the **stretching** (solid lines) and bending (dashed lines) energy fractions are shown; the shear and torsional modes carry less than 5% of the total energy at any stage of the deformation history.

3.3 Physical origins of the reinforcement effect

Three hypotheses regarding the physical origins of the reinforcement effect are analyzed in this section. We first analyze the hypothesis that reinforcement is due to the fact that fillers act as additional network cross-links with high connectivity. The second hypothesis relates to the excluded volume effect, i.e. the requirement that fibers do not overlap other fibers and do not penetrate fillers during deformation. The third hypothesis is based on the idea that fillers constrain

the deformation of the network, with the degree of confinement increasing as the wall-to-wall distance between fillers decreases.

3.3.1 Connectivity hypothesis

The stiffness of fiber networks depends markedly on the mean nodal connectivity, \bar{z} [21]. Increasing \bar{z} may also cause a transition from the bending-dominated to the stretching-dominated deformation mode. In filled networks, each filler comes in contact with many fibers and may be thought as a network node with excluded volume and large z . Hence, it is of interest to inquire to what extent the observed reinforcement is associated with the increase of the effective average z of the network.

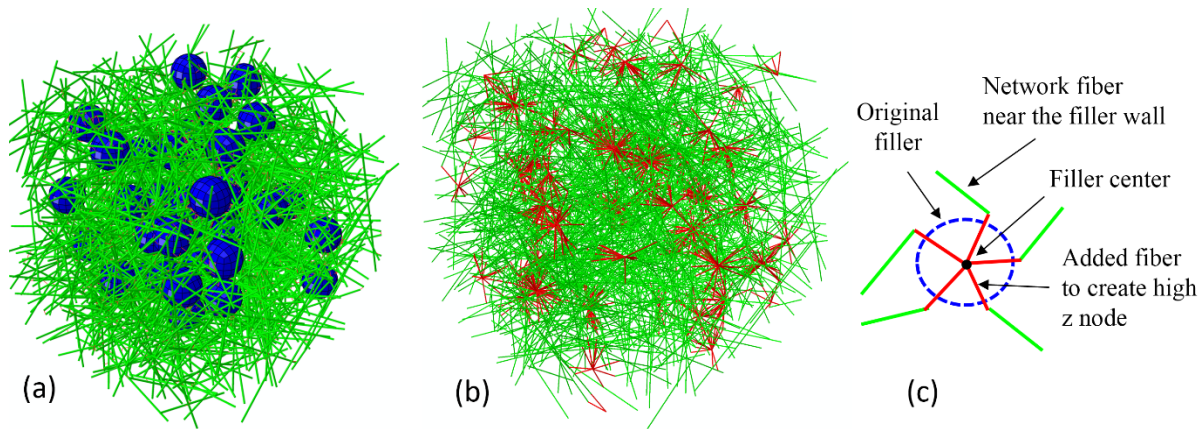


Figure 7. (a) Original filled network with $\phi=5\%$, (b) equivalent network with high z nodes where each filled is replaced by additional fiber segments (red lines) connecting the neighboring network fibers (green lines) to the filler center, and (c) a schematic illustrating how additional fiber segments are introduced to create the high z node for each filler (color online).

To clarify this issue, we consider filled networks in which fillers are replaced by high z nodes as shown in Figure 7. Figure 7(a) shows the original filled network with $\phi=5\%$ whereas Figure 7(b) illustrates the equivalent network with high z nodes. Specifically, each filler is replaced by fiber segments (red lines in Figure 7(b)) continuing the fibers that come in contact with the respective filler surface to a node located at its geometric center, as illustrated in Figure 7(c). The connectivity number of this node, z , is equal to the number of fibers in contact with the respective filler. The fiber segments added in this process have the same **stretching** and bending rigidity as all other

fibers of the network. Since fillers are effectively removed via this procedure, the excluded volume constraint they impose is eliminated.

Figure 8(a) shows stress-stretch curves for a filled network with $l_b/L_0 = 8 \times 10^{-3}$ and $\phi = 5\%$, for the equivalent unfilled network and for the network in which fillers are replaced by high z nodes. The curve corresponding to the modified network with high connectivity overlaps that of the unfilled network and does not exhibit the reinforcement observed in the actual filled network case. The modified network has higher \bar{z} compared with the unfilled network, but the difference is small, given that there are many more regular network nodes per unit volume than high z nodes. Figure 8(b) shows the energy partition in these three types of structures. Once, again, the energy partition in the network with high z nodes is quite similar to that of the unfilled, reference network. We conclude that this mechanism is not responsible for the observed reinforcement in filled networks.

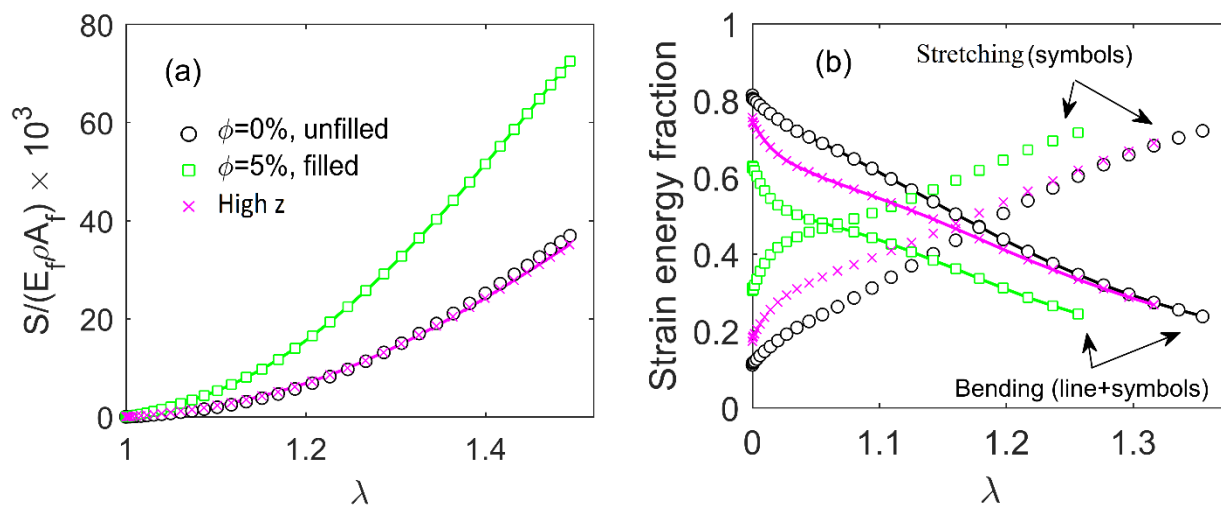


Figure 8. (a) Comparison of stress-stretch curves for a filled network with $l_b/L_0 = 8 \times 10^{-3}$ and $\phi = 5\%$ (filled), the corresponding unfilled network (unfilled) and the network that results from the filled one by replacing fillers with nodes of high connectivity (high z). The vertical axis is normalized with the density of the network in order to compensate for the density variation associated with the substitution of high z nodes for fillers. (b) Energy partition for the three cases in (a).

3.3.2 Excluded volume hypothesis

It is of interest to inquire to what extent the excluded volume condition (the fact that fibers cannot cross each other and cannot penetrate fillers) is responsible for the observed reinforcement.

To clarify this issue, we compare in Fig. 9 stress-stretch curves for networks with $l_b/L_0 = 8 \times 10^{-3}$, and $\phi = 5\%$ and 10% , obtained with and without enabling the contact constraints during simulation. The data indicates that contacts make little contribution to the overall mechanical response in tension. This is due to the large free volume of the network. Contacts become slightly more important in shear and are essential in compression [27,48]. We conclude that reinforcement is not directly associated with the occurrence of inter-fiber, fiber-filler or filler-filler contacts in the effect observed here in uniaxial tension. The excluded volume of fillers is expected to become important at large filling fractions, but these situations are of importance in a limited number of practical applications.

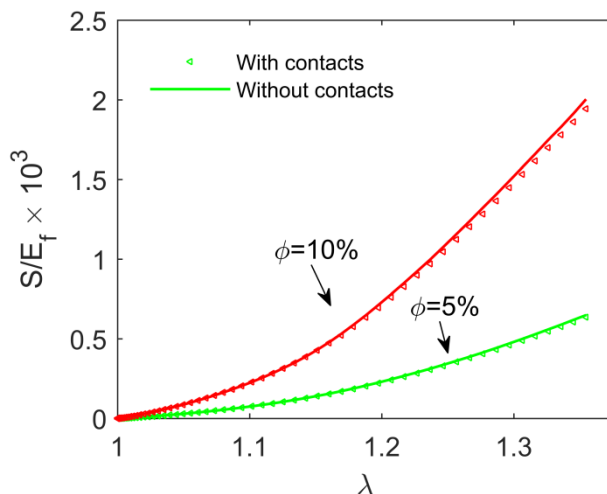


Figure 9. Stress-stretch curves for networks with $l_b/L_0 = 8 \times 10^{-3}$ and $\phi = 5\%$ and 10% obtained with and without the excluded volume constraint.

3.3.3 Confinement hypothesis

To explore the effect of confinement, we modify the size of inclusions at constant ϕ ($\phi = 5\%$), from $D = 2l_c$ to $D = 3l_c$. This leads to an increase of the average wall-to-wall distance between fillers, ω , from $\omega/l_c = 2.8$ to $\omega/l_c = 4.2$. Figure 10(a) shows the stress-stretch curves for the unfilled network with $l_b/L_0 = 8 \times 10^{-3}$, and for the filled network with $\phi = 5\%$ with two values

of D . Increasing the wall-to-wall distance decreases the degree of confinement, which has a strong effect on reinforcement. The curve corresponding to the large ω/l_c value is close to that of the unfilled network. Figure 10(b) shows the energy partition for all cases presented in Fig. 10(a). Once again, increasing ω/l_c brings the filled network closer to the situation of the unfilled network, promoting the bending dominated deformation and postponing to larger strains the transition to **stretching** dominance. It results that the effects discussed in this article originate from the confinement imposed by fillers on the surrounding network which restricts the softer bending deformation mode of fibers and promotes the stiffer **stretching** mode.

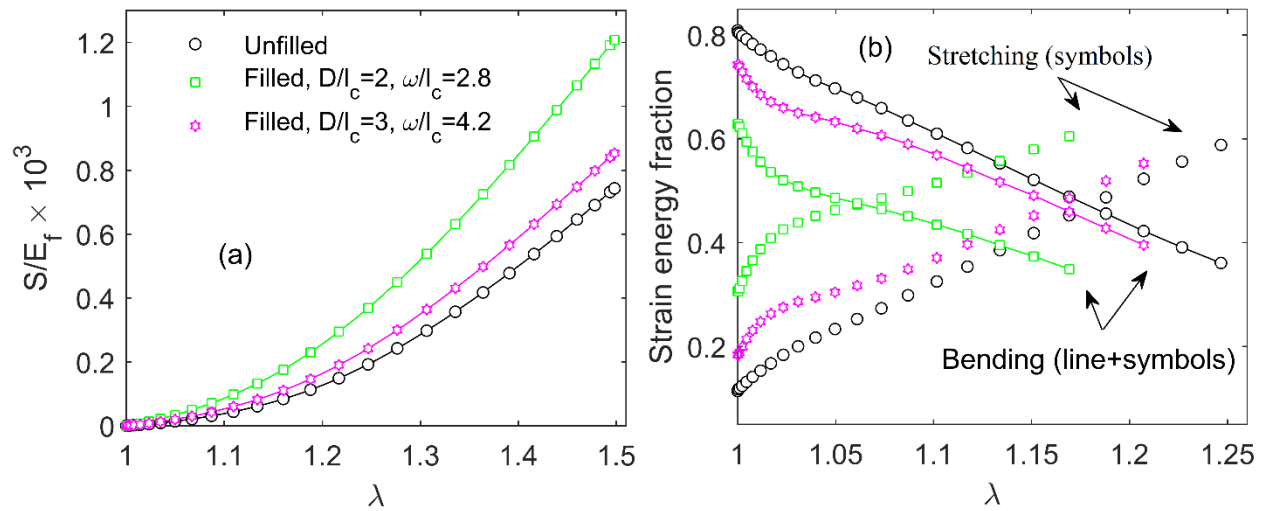


Figure 10. (a) Stress-stretch curves for the unfilled network with $l_b/L_0 = 8 \times 10^{-3}$ and two filled networks with $\phi = 5\%$ and filler diameter $D/l_c = 2$ and 3, respectively. (b) Energy partition for the three cases shown in (a).

3.4 Fillers reduce the Poisson effect

Networks with large free volume, which are not embedded in a continuum matrix, exhibit large Poisson contraction when subjected to uniaxial tension [49-51]. This is due to the reorientation of filaments in the loading direction during regime II of deformation (Fig. 2(a)). The same non-linear mechanism causes the Poynting effect under shear loading [52]. Figure 11(a) shows the incremental Poisson ratio of unfilled and a series of filled networks with $l_b/L_0 = 8 \times 10^{-3}$ and increasing ϕ . The incremental Poisson ratio is computed as

$$\nu_i = -\frac{d(\ln(\lambda_l))}{d(\ln(\lambda))}$$

where λ and λ_l are stretches in the loading and transverse directions, respectively. The incremental Poisson ratio ν_i reduces to the conventional Poisson ratio, ν_0 , at infinitesimal strains. The unfilled network exhibits a rapid increase of ν_i during regime II (marked by arrows). A maximum is reached towards the end of regime II, beyond which ν_i decreases. The origin of this behavior is discussed in [51]. Filled networks exhibit similar trends, but the maxima of the respective curves decreases as ϕ increases.

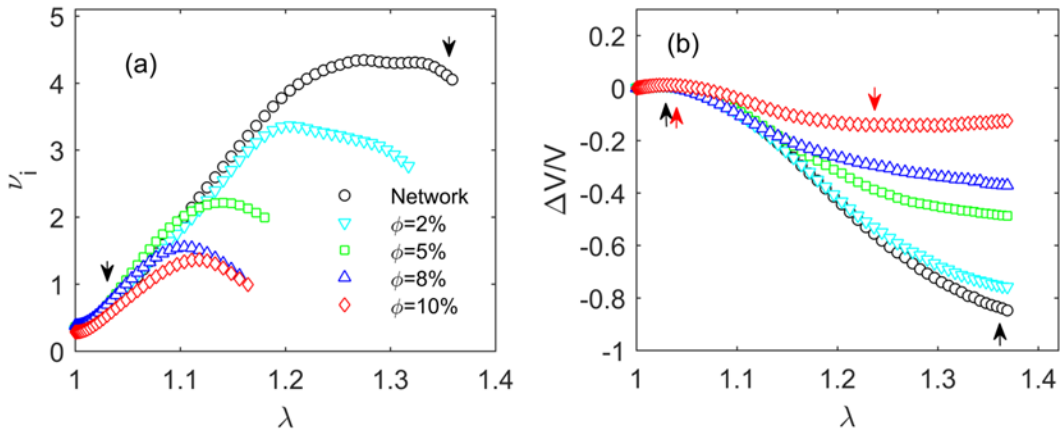


Figure 11. (a) Variation of the incremental Poisson ratio of the unfilled network with $l_b/L_0 = 8 \times 10^{-3}$ and of filled networks with various ϕ . The corresponding volumetric strains are shown in (b). The arrows indicate transitions between regimes I and II, and regimes II and III, respectively (see also Fig. 2), for the unfilled network and for the filled network with $\phi = 10\%$.

Figure 11(b) shows the variation of the model volume relative to the volume of the unloaded model for all cases shown in Fig. 11(a). The strong volume reduction observed during regime II is associated with the large increase of the incremental Poisson ratio (Fig. 11(a)). The volume reduction decreases in magnitude as ϕ increases and for $\phi = 10\%$ the network volume is almost constant during deformation. This demonstrates that the constraints imposed by fillers on the deformation of the surrounding network lead to deformation conditions closer to isochoric even in presence of a large free volume in the network. This can be understood based on the observation that fillers render the deformation more **stretching-dominated**. Unfilled **stretching-dominated** (and therefore almost affinely-deforming) networks exhibit much weaker Poisson effect than the equivalent bending-dominated networks. Figure 12 shows corresponding deformed and

undeformed networks with $\phi = 0\%, 5\%, 10\%$, respectively, demonstrating the reduction of the Poisson effect associated with the presence of fillers.

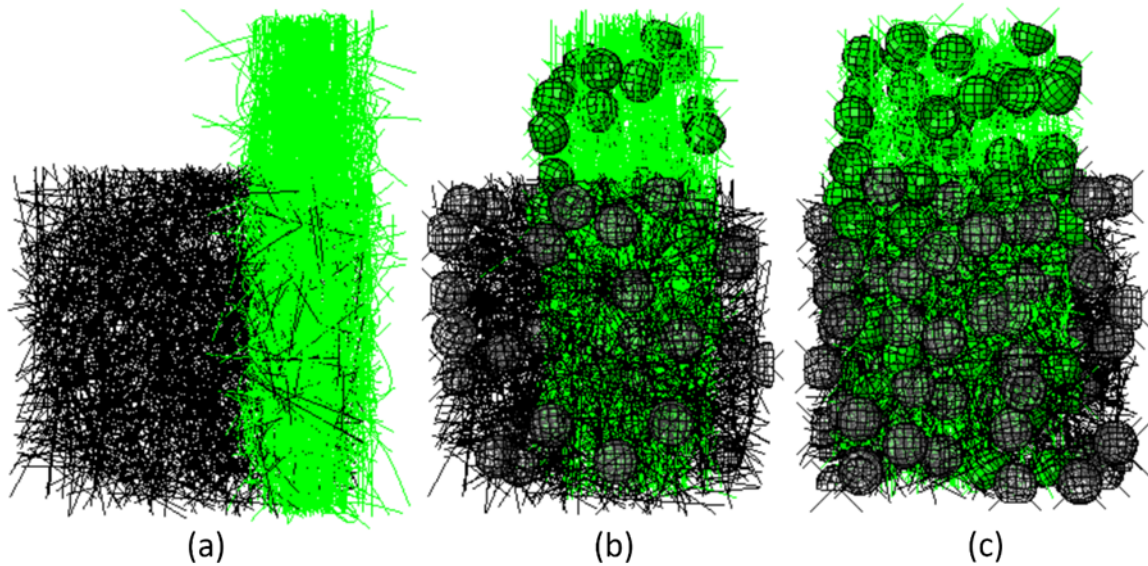


Figure 12. Deformed (green) model configurations of (a) unfilled network, (b) filled network with $\phi=5\%$ and (c) filled network with $\phi=10\%$. Undeformed configurations (black) are overlaid to demonstrate the reduction of the Poisson effect in the presence of inclusions.

3.5 Non-bonded filler-network interfaces

A related perspective on the constraints imposed by fillers on network deformation can be obtained by modifying the state of the filler-network interface. In all cases discussed above, fibers are connected to fillers through ‘welded’ bonds that transmit both forces and moments. We gradually relax these constraints to investigate their relative effect on confinement and reinforcement. In the first stage, the fiber-filler bonds are represented as ‘pin joints,’ which transmit only forces. Figure 13 shows the stress-stretch curves for the filled network with $l_b/L_0 = 8 \times 10^{-3}$ and $\phi = 5\%$, and with ‘welded’ and ‘pin-jointed’ network-filler bonds. Reducing the kinematic constraint at the filler-network interface causes a significant reduction of the reinforcement. Taking one step further and removing all bonds between fillers and the network, while insuring that fibers do not penetrate fillers (state denoted by ‘unbonded’) leads to an even more drastic reduction of reinforcement. Note that the curve for this last case falls below that of the unfilled network (Fig. 13). In fact, the filled network with unbonded interfaces may be compared with a network in which inclusions are

replaced by spherical holes of same size and same total volume fraction with the fillers. This network (denoted by ‘porous’) is obviously softer than the unfilled network. This is seen in Fig. 13, where the curves for the ‘unbonded’ and ‘porous’ cases overlap. This observation re-emphasizes the results discussed in section 3.3.2 which indicate that excluded volume effects are weak in these networks subjected to uniaxial tension.

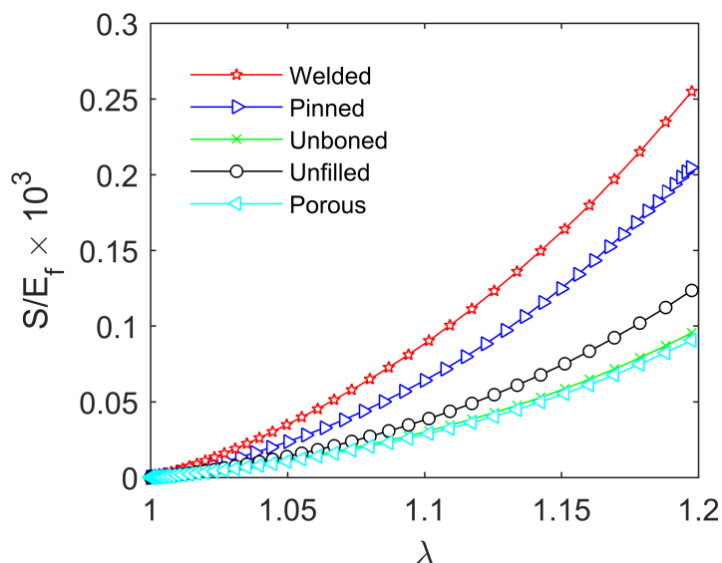


Figure 13. Stress-stretch curves for the filled network with $l_b/L_0 = 8 \times 10^{-3}$ and $\phi = 5\%$, and with various states of the filler-network interface: ‘welded’ and ‘pinned’ correspond to fiber-filler bonds that transmit both forces and moments, and only forces, respectively. ‘Unbonded’ corresponds to models in which there are no bonds between fibers and fillers, but the excluded volume constraint is imposed. ‘Porous’ corresponds to a system in which fillers are replaced by holes.

Finally, it is of interest to discuss the role of the assumption that fillers are rigid. While the rigid case is an appropriate representation for most polymeric nanocomposites, biological networks generally embed soft, but (generally) volume preserving inclusions. Examples include cell-seeded biopolymer networks and artificial tissue scaffolds, and platelet-reinforced fibrin clots. This case requires a separate study. However, based on the present results it can be conjectured that reducing the stiffness of fillers would decrease the reinforcement effect because the constraint imposed by fillers on fibers would be partially relaxed. Since here we observe that the excluded volume constraint has a weak impact on reinforcement, we expect the condition that inclusions volume remains constant to have a weak or no effect on the overall filled network behavior.

4. Conclusions

The mechanical behavior of cross-linked athermal fiber networks embedding rigid spherical inclusions is investigated in this work. Inclusions increase the small strain network stiffness, but reduce the strain stiffening ability of the network at larger strains, in the non-linear regime. Reinforcement depends on the nature of the network, being pronounced in networks which are bending-dominated in the unfilled state, and rather weak in networks which are [stretching-dominated](#) when unfilled. The effect is associated with the kinematic restrictions imposed by fillers on fibers in their vicinity. This confinement promotes the much stiffer [stretching](#) deformation mode of fibers. A gradual transition from bending-dominated to stretching-dominated deformation is observed as the filling volume fraction increases. Decreasing the wall-to-wall distance between inclusions, while maintaining the filling fraction constant, enhances the reinforcement effect and promotes the [stretching](#) deformation mode of the network. Further, inclusions restrict fiber reorientation during loading and limit the overall Poisson effect. These results shed light on the physical basis of reinforcement in a number of material systems of high practical interest.

Acknowledgment

This work was supported in part by the NSF through grant No. CMMI-1634328.

References

- [1] P. A. Janmey, *Current opinion in cell biology* **3**, 4 (1991).
- [2] R. H. Pritchard, Y. Y. Huang, and E. M. Terentjev, *Soft Matter* **10**, 1864 (2014).
- [3] M. R. Islam, G. Tudryn, R. Bucinell, L. Schadler, and R. C. Picu, *Sci Rep* **7**, 13070 (2017).
- [4] M. Alava and K. Niskanen, *Reports on progress in physics* **69**, 669 (2006).
- [5] C.-L. Pai, M. C. Boyce, and G. C. Rutledge, *Polymer* **52**, 6126 (2011).
- [6] O. Yeoh, *Rubber chemistry and technology* **63**, 792 (1990).
- [7] W. H. Rombouts, M. Colomb-Delsuc, M. W. T. Werten, S. Otto, F. A. de Wolf, and J. van der Gucht, *Soft Matter* **9**, 6936 (2013).
- [8] W.-C. Lin, W. Fan, A. Marcellan, D. Hourdet, and C. Creton, *Macromolecules* **43**, 2554 (2010).
- [9] Y. Cao, Y. Zhou, Y. Shan, H. Ju, and X. Xue, *Adv. Mater.* **18**, 1838 (2006).
- [10] C. Xu, W. Lu, S. Bian, J. Liang, Y. Fan, and X. Zhang, *The Scientific World Journal* **2012** (2012).
- [11] R. J. Kane, H. E. Weiss-Bilka, M. J. Meagher, Y. Liu, J. A. Gargac, G. L. Niebur, D. R. Wagner, and R. K. Roeder, *Acta Biomater.* **17**, 16 (2015).
- [12] M. R. Islam, G. Tudryn, R. Bucinell, L. Schadler, and R. C. Picu, *Journal of Materials Science* **53**, 16371 (2018).
- [13] R. C. Picu, *Soft Matter* **7**, 6768 (2011).
- [14] C. P. Broedersz and F. C. MacKintosh, *Reviews of Modern Physics* **86**, 995 (2014).
- [15] M. J. Unterberger and G. A. Holzapfel, *Biomech Model Mechanobiol* **13**, 1155 (2014).
- [16] F. C. MacKintosh, J. Kas, and P. A. Janmey, *Phys. Rev. Lett.* **75**, 4425 (1995).
- [17] J. C. Maxwell, *Philos. Mag.* **27**, 250 (1864).
- [18] D. A. Head, A. J. Levine, and F. MacKintosh, *Physical review letters* **91**, 108102 (2003).
- [19] A. S. Shahsavari and R. C. Picu, *Physical Review E* **86**, 011923 (2012).
- [20] R. Connelly and W. Whiteley, *SIAM Journal on Discrete Mathematics* **9**, 453 (1996).
- [21] A. Sharma, A. Licup, R. Rens, M. Vahabi, K. Jansen, G. Koenderink, and F. MacKintosh, *Physical Review E* **94**, 042407 (2016).
- [22] J. Wilhelm and E. Frey, *Physical review letters* **91**, 108103 (2003).
- [23] S. Bancelin, B. Lynch, C. Bonod-Bidaud, G. Ducourthial, S. Psilodimitrakopoulos, P. Dokládal, J.-M. Allain, M.-C. Schanne-Klein, and F. Ruggiero, *Scientific reports* **5**, 17365 (2015).
- [24] G. A. Holzapfel, *The handbook of materials behavior models* **3**, 1049 (2001).
- [25] P. R. Onck, T. Koeman, T. van Dillen, and E. van der Giessen, *Phys Rev Lett* **95**, 178102 (2005).
- [26] C. Storm, J. J. Pastore, F. C. MacKintosh, T. C. Lubensky, and P. A. Janmey, *Nature* **435**, 191 (2005).
- [27] M. R. Islam and R. C. Picu, *Journal of Applied Mechanics* **85**, 081011 (2018).
- [28] P. Bursac, G. Lenormand, B. Fabry, M. Oliver, D. A. Weitz, V. Viasnoff, J. P. Butler, and J. J. Fredberg, *Nature materials* **4**, 557 (2005).
- [29] Y. L. Han, P. Ronceray, G. Xu, A. Malandrino, R. D. Kamm, M. Lenz, C. P. Broedersz, and M. Guo, *Proc. Natl. Acad. Sci. U.S.A.* **115**, 4075 (2018).
- [30] D. G. Papageorgiou, I. A. Kinloch, and R. J. Young, *Prog. Mater. Sci.* **90**, 75 (2017).
- [31] M. Islam, G. J. Tudryn, and R. C. Picu, *Comput. Mater. Sci.* **125**, 309 (2016).
- [32] S. Deogekar and R. C. Picu, *Physical Review E* **95**, 033001 (2017).
- [33] C. Heussinger and E. Frey, *Eur. Phys. J. E* **24**, 47 (2007).

- [34] D. A. Head, A. J. Levine, and F. C. MacKintosh, *Physical review. E, Statistical, nonlinear, and soft matter physics* **68**, 061907 (2003).
- [35] S. Nemat-Nasser and M. Hori, *Micromechanics: overall properties of heterogeneous materials* (Elsevier, Newyork, NY,USA, 2013).
- [36] P. Wutticharoenmongkol, N. Sanchavanakit, P. Pavasant, and P. Supaphol, *Macromol. Biosci.* **6**, 70 (2006).
- [37] N. Domun, H. Hadavinia, T. Zhang, T. Sainsbury, G. Liaghat, and S. Vahid, *Nanoscale* **7**, 10294 (2015).
- [38] A. Version, Dassault Systemes Simulia Corp., Providence, RI (2013).
- [39] X. F. Wu and Y. A. Dzenis, *Journal of Applied Physics* **98**, 093501 (2005).
- [40] L. M. Jawerth, Harvard University, 2013.
- [41] R. M. Christensen, *J. Mech. Phys. Solids* **38**, 379 (1990).
- [42] K. Berkache, S. Deogekar, I. Goda, R. Picu, and J.-F. Ganghoffer, *Composite Structures* **181**, 347 (2017).
- [43] A. S. Shahsavari and R. C. Picu, *Physical Review E* **92**, 012401 (2015).
- [44] M. Bai, A. R. Missel, W. S. Klug, and A. J. Levine, *Soft Matter* **7**, 907 (2011).
- [45] E. M. Huisman, C. Heussinger, C. Storm, and G. T. Barkema, *Phys Rev Lett* **105**, 118101 (2010).
- [46] A. J. Licup, S. Münster, A. Sharma, M. Sheinman, L. M. Jawerth, B. Fabry, D. A. Weitz, and F. C. MacKintosh, *Proc. Natl. Acad. Sci. U.S.A.* **112**, 9573 (2015).
- [47] G. Žagar, P. R. Onck, and E. Van der Giessen, *Macromolecules* **44**, 7026 (2011).
- [48] H. X. Zhu, N. J. Mills, and J. F. Knott, *J. Mech. Phys. Solids* **45**, 1875 (1997).
- [49] D. Vader, A. Kabla, D. Weitz, and L. Mahadevan, *PloS one* **4**, e5902 (2009).
- [50] A. Kabla and L. Mahadevan, *J. Royal Soc. Interface* **4**, 99 (2007).
- [51] R. C. Picu, S. Deogekar, and M. R. Islam, *Journal of biomechanical engineering* **140**, 021002 (2018).
- [52] P. A. Janmey, M. E. McCormick, S. Rammensee, J. L. Leight, P. C. Georges, and F. C. MacKintosh, *Nature materials* **6**, 48 (2007).